TG-983
MARCH 1968
Copy No

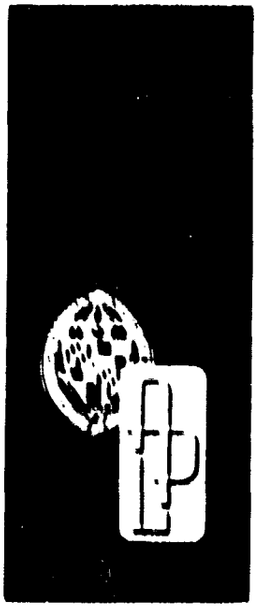

AD638135

Technical Memorandum

STATISTICAL ANALYSIS OF TEMPERATURE DATA FROM WIND TUNNEL TEST OF A VON KARMAN RADOME

by M. B. TATE

DDC
RECEIVED
APR 29 1968

[illegible] UNIVERSITY • APPLIED PHYSICS LABORATORY

This document has been approved for public release and sale; its distribution is unlimited

29

DISCLAIMER NOTICE

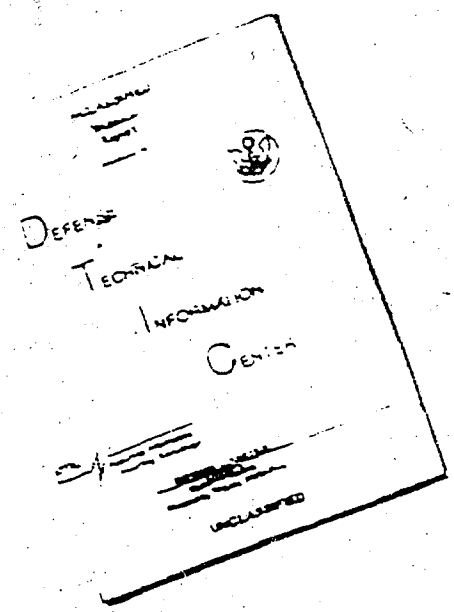

THIS DOCUMENT IS BEST QUALITY AVAILABLE. THE COPY FURNISHED TO DTIC CONTAINED A SIGNIFICANT NUMBER OF PAGES WHICH DO NOT REPRODUCE LEGIBLY.

THIS DOCUMENT CONTAINED BLANK PAGES THAT HAVE BEEN DELETED

REPRODUCED FROM BEST AVAILABLE COPY

TG-983
MARCH 1969
Copy No.

Technical Memorandum

STATISTICAL ANALYSIS OF TEMPERATURE DATA FROM WIND TUNNEL TEST OF A VON KARMAN RADOME

by M. B. TATE

THE JOHNS HOPKINS UNIVERSITY • APPLIED PHYSICS LABORATORY
8621 Georgia Avenue, Silver Spring, Maryland 20910
Operating under Contract NOw 62-0604-c with the Department of the Navy

This document has been approved for public release and sale; its distribution is unlimited

THE JOHNS HOPKINS UNIVERSITY
APPLIED PHYSICS LABORATORY
SILVER SPRING, MARYLAND

ABSTRACT

Temperatures obtained from an Ordnance Aerophysics Laboratory wind-tunnel test on a Von Karman radome are studied and put into functional form for theoretical analysis of radome thermal stresses. It was found that the radome wall temperature can be expressed analytically by a single function that defines the temperatures at all points in the wall except for a short length near the tip, for which another expression is developed. The single function can be further separated by variables into two functions, one of which describes the spanwise distribution and the other the wall-thickness distribution of the temperature. This finding is highly advantageous mathematically.

The analytical and test results are presented and compared in Figures 1, 2, and 3 and recorded in two tables. Good agreement between experiment and analysis was found to exist, with the difference range generally not in excess of approximately ±7 percent while being less than half this amount in most cases. The derived function overestimates the maximum temperatures by about 0.5 percent, but this is a conservative feature insofar as the theoretical prediction of thermal stress is concerned. The range of experimental error in the original data was reported by the test engineers also to be about ±7 percent.

PRECEDING
PAGE BLANK

THE JOHNS HOPKINS UNIVERSITY
APPLIED PHYSICS LABORATORY
SILVER SPRING MARYLAND

TABLE OF CONTENTS

PRECEDING
PAGE BLANK

THE JOHNS HOPKINS UNIVERSITY
APPLIED PHYSICS LABORATORY
SILVER SPRING MARYLAND

LIST OF ILLUSTRATIONS

PRECEDING
PAGE BLANK

INTRODUCTION

The current investigation of radome thermal stresses has been conducted by seeking solutions to a sequence of problems upon which the final solution depends. The early studies dealt with the nosecap behavior and can be identified through the bibliography of Reference (b), and the general theory for the radome wall behavior is developed in Reference (b). Auxiliary investigations on normal stress and moment factors, second-order stiffness functions, and elastic-axis location are referenced also in (b). From these studies, it was learned that the theory is amenable to numerical evaluation of the bending-moment, normal-stress, and shearing-stress resultants, and the stresses and displacements. All of these quantities bear directly on the overall solution in the critical respect that the absence of any one of them prevents the determination of various unknowns, without which no definite solution for the thermal stresses can be obtained.

After it was learned that the above mentioned problems could be coped with, the thermoelastic mechanical properties of the radome construction material were examined in Reference (c). Therein it was discovered that these properties can be treated analytically, or, if such treatment should prove to be too cumbersome, they can be handled by certain carefully defined numerical techniques for integration and differentiation.

We then heard that everyone involved desired to see the theoretical solutions correlated with OAL* tests that were carried out on Von Karman radomes. Since the Von Karman radome is a markedly different structure than any of those for which theoretical solutions have been evolved, the geometric characteristics were examined in Reference (d). It is shown in (d) that both principal radii of curvature vanish at the tip of a Von Karman radome and the major one vanishes at the base. These characteristics can lead to infinite discontinuities in the stress and moment formulas if one fails to introduce suitable restrictions in advance. If such restrictions turn out to be unavailable, the analyst must provide functional continuity by another means which will be discussed subsequently when appropriate.

Furthermore, the Von Karman shape possesses aerodynamic characteristics at all Mach numbers that are absent or negligible in the usual missile cones and ogives above Mach 2. The effect on the temperature distribution can be observed

* OAL = Ordnance Aerophysics Laboratory, General Dynamics.

in Figures 2 and 3 herein near the tip of the test radome. The phenomenon is caused by a transonic zone* embedded in the flow field between a detached shock wave and the blunt tip, and it has a suprisingly large effect on the maximum temperatures in the first inch or so of length measured from the tip of the radome. To prepare for this contingency, the previous investigation (Reference (a)) was undertaken. It proved to be tedious, but its conclusion was gratifyingly fruitful in the excellent correlation that it has led to in this report.

NOMENCLATURE

A,B:	Constants
F:	Fahrenheit
M:	Mach number
R:	Radius, inches
T:	Temperature, °F or °R
V:	Velocity, fps
Z:	Geometric axis of radome
c:	Half thickness of radome shell wall c=h/2, inches; specific heat
f:	Function
h:	Wall thickness of radome shell, inches
k:	Coefficient of thermal conductivity, Btu/ft-hr-°F
ℓ:	Length, inches
i,n:	Positive integers; 1,2,3,....
p:	Pressure, psi or psf
t:	Time, seconds
v:	Volume, cubic inches
x:	Wall-thickness variable ratio, x=y/c
y:	Wall thickness variable, inches
z:	Coordinate along Z-axis, inches
γ:	Specific heat ratio, c_p/c_v (γ = 1.4 for air)
ψ:	Coordinate angle, degrees or radians

* See footnote below equation (1) in the text section entitled "Temperature Distribution".

The following symbols appear as subscripts:

a:	Values at outer surface "a"
c:	Values at central surface "c"
n,i:	Numerical indices
o:	Free-stream properties; origin or initial (zero)
p:	Pressure
s:	Values at inner surface "s"
t:	Total--in reference to total temperature; thermal
v:	Volume

TEMPERATURE DISTRIBUTION

It was shown in Reference (a) that temperatures along the exterior surface of a blunt radome in the transonic zone* can be represented by

$$T_a = T_{ao} - \sin^2\psi \ (A_o + A_1 \sec^2\psi - A_2 \cos^2\psi)^2 \qquad (1)$$

where T_a is located along the radome's outer surface by the coordinate angle ψ, which is defined and illustrated in References (a), (b), and (d), while two specific values are shown in the sketch herein at the top of Figure 3. And the temperature at the tip ($\psi=0$), or leading edge, of the radome is denoted by T_{ao} as indicated by equation (1).

After the air mass moves beyond the transonic zone, the surface temperature can be represented by

$$T_a = T_{ao} - \sin^2\psi (B_o - B_2 \cos^2\psi)^2 \qquad (2)$$

where, in general, the constants A_i and B_i in equations (1) and (2) cannot be computed directly, but they can be found from experimental data or numerical analyses, as is illustrated in Figures 1, 2, and 3.

* This terminology is defined in Reference (e), p. 270; i.e., a supersonic free stream approaches a blunt body and is reduced to a subsonic flow by passing through a detached shock wave. As the flow continues in the zone between the shock wave and the blunt nose, its speed increases to again become supersonic. The flow is called transonic if both subsonic and supersonic regions are present in the field.

In Figure 1, part of the plotted data was reported in References (f) and (i), while a computer program for the remainder was described in Reference (h) with the applicable results listed in Table 4 on Figure 4 in Appendix A of the present report. The temperatures in Table 4 on Figure 4 were computed as constant, or average, values in the segmental volumes shown in Figure 4. These averages are plotted in Figure 1 at the thermal-mass-centers of the volume elements discussed in Appendix A. A thermal-mass-center (located by $\bar{x}_t$) differs from the volume-element centroid owing to the temperature variant coefficient of thermal conductivity (k) of the wall material, which was Pyroceram 9606 in the test radome. Necessary formulas for the thermal-mass-center computations are given in Appendix A where also the variable k-values are listed in Table 3. The centers were calculated for interior elements (Figure 4) at $\bar{x}_t = -0.751$; the second row from the interior, at $\bar{x}_t = -0.248$ to -0.253; the row above the center line, from $\bar{x}_t = +0.247$ to $+0.253$; and the top row of elements was found to lie at approximately $\bar{x}_t = +0.90$.

The regression equations developed from the analytical and experimental data for the cross sections shown in Figure 1 have the general form

$$(T)_{\psi=\psi_i} = \sum_{n=o}^{3} T_{ni}x^n = T_c + T_{1\,i}x + T_{2\,i}x^2 + T_{3\,i}x^3 \qquad (3)$$

wherein $T_c = T_c(\psi)$ is the spanwise function for the temperature distribution along the central surface of the radome wall, and $x=y/c$ is the wall-thickness variable ratio, which is illustrated in the upper right-hand corner of Figure 1. The remaining T_{ni} are coefficients that vary with the spanwise (ψ-dependent) location of each cross section of the wall as denoted by the index "i". Exemplification of their magnitudes is furnished by the formulas that follow.

$$(T)_{\psi=o} = 352 + 482x + 388x^2 + 98x^3 \qquad (4)$$

$$(T)_{\psi=61°37'42''} = 239 + 337x + 295x^2 + 85x^3 \qquad (5)$$

$$(T)_{\psi=62°02'} = 238 + 335x + 294x^2 + 84x^3 \qquad (6)$$

$$(T)_{\psi=63°43'59''} = 231 + 325x + 284x^2 + 81x^3 \qquad (7)$$

$$(T)_{\psi=65°04'03''} = 226 + 318x + 276x^2 + 78x^3 \qquad (8)$$

$$(T)_{\psi=66°13'} = 223 + 312x + 270x^2 + 76x^3 \qquad (9)$$

$$(T)_{\psi=83°27'35''} = 182 + 236x + 186x^2 + 45x^3 \qquad (10)$$

After finding the surface temperatures by regression analysis of the cross-sectional distributions discussed above in connection with Figure 1, the constants (T_{ao}, B_o, and B_2) of equation (2) were calculated statistically to obtain

$$T_a = 1319 - (26.34-20.53\cos^2\psi)^2\sin^2\psi, \quad 61°37'42'' \leq \psi \leq 90° \qquad (11)$$

which is shown in Figure 2 along with the plotted data employed in the calculations. Furthermore, in order to furnish an illustration of the application of equation (1), the A_i were computed from the diamond-shaped data points (Figure 2) that are plotted in the first inch of the radome length measured from the tip. Through the boundary layer along the outer surface of the radome, air-flow and heat-exchange calculations are carried out by using appropriate Reynold's numbers with laminar flow followed by a transition to turbulent flow over the region affected by the transonic zone between the shock wave and the radome surface, which produces the circumstances wherein equation (1) is applicable. Two expressions were used to meet therequirements in the first inch from the tip, and they are

$$T_a = 1319 - (91.16 - 11.13\sec^2\psi - 78.60\cos^2\psi)^2\sin^2\psi, \quad 0 \leq \psi \leq 53°41'17'' \qquad (12)$$

$$T_a = 1319 - (203.4 - 27.49\sec^2\psi - 205.05\cos^4\psi)^{1/2}\sin^2\psi, \quad 51°41'17'' \leq \psi \leq 61°37'42'' \tag{11}$$

where equations (11) to (13), inclusive, provide analytical description of the surface temperature (T_a) along the entire span (28.1 inches) from $\psi=0$ to 90°.

To secure central-surface and inner-surface spanwise distributions of wall temperatures (T_c and T_s respectively), the values calculated with equations (4) to (10) together with the analytical and experimental data reported in Reference (1) were plotted on Figure 3. For air flows of sufficient duration (the test time in the present instance is four seconds, which is probably more than sufficient), one can anticipate that spanwise distributions of temperature along the surfaces in the radome wall that are parallel to the exterior surface can also be described by equations similar to (1) and (2). The expectation is verified by the regression curves drawn on Figure 3 for the exterior, central, and interior surfaces of the wall of the test radome. These formulas apply in the interval $61°37'42'' \leq \psi \leq 90°$:

$$T_a = 1319 - (26.34 - 20.53\cos^2\psi)^{1/2}\sin^2\psi \tag{14}$$

$$T_c = 352 - (13.19 - 4.79\cos^2\psi)^{1/2}\sin^2\psi \tag{15}$$

$$T_s = 160 - (8.639 - 3.013\cos^2\psi)^{1/2}\sin^2\psi \tag{16}$$

and the curve for the last one, equation (16), passes through the two data points at 1.75 and 24 inches from the tip (Figure 3) where temperatures were measured directly in the OAL wind-tunnel tests. These measurements represent the best current verification of information that we have on the radome temperatures.

The temperature distribution through the thickness of a radome wall is defined by

$$T = \sum_{n=0}^{n'} T_n x^n \tag{17}$$

where $T = T(\psi, x)$ is the temperature at any point in the wall if n' is the same for all cross sections and the T_n are functions of ψ, such as T_a, T_c, T_s of equations (14) to (16). It was learned from the analytical and experimental data studied and reported herein that the foregoing concept is substantially realized in the tested radome and $n' = 3$. Hence, equation (17) may be written as

$$T = \sum_{n=0}^{3} T_n x^n = T_c + T_1 x + T_2 x^2 + T_3 x^3 \tag{18}$$

where the initial function (T_c) is given by equation (15) and the remaining T_n are

$$T_1 = (T_a + 4T_c - 5T_s)/4 \tag{19}$$

$$T_2 = (T_a - 2T_c + T_s)/2 \tag{20}$$

$$T_3 = (T_a - 4T_c + 3T_s)/4 \tag{21}$$

wherein the three functions on the right-hand side in each of the above formulas are given by equations (14), (15), and (16) for the outer, central, and inner surface spanwise distributions of temperature.

It is a very real advantage from an analytical viewpoint of thermal-stress analysis when the temperature (T) at any point in the radome wall can be represented by separable functions of ψ and x. Toward this end, the previous results were examined, and a fully satisfactory function was derived from them; e.g.,

$$T = T_a f(x) \tag{22}$$

where the f(x) is given by

$$f(x) = 0.257 + 0.358x + 0.305x^2 + 0.084x^3 \tag{23}$$

and T_a is the outer surface temperature function of equation (14). In the forward part of the radome where the most serious thermal conditions prevail, the use of

equation (22) overestimates the maximum temperatures by less than one-half percent; temperatures along the central surface are obtained within +1 to -4 percent, and the inner surface values within about one percent. At 24 inches from the tip, the exterior surface temperature is overestimated by about one-half percent, and values inside the wall are found to be from approximately six to ten percent less than those plotted on Figure 1-e. But, since most of these differences tend toward conservatism in the analysis of thermal stresses, they are considered acceptable.

The computed temperatures and other necessary data are tabulated to permit further comparisons as well as for future reference purposes. Therefore, the test radome coordinates are listed in Table 1, and the temperature data are summarized in Table 2.

DISCUSSION

The results of this investigation are presented in Figures 1, 2, and 3 and Tables 1 and 2. In general, they are based on the experimental and analytical information reported in References (f) and (i) together with data from the computer program described in Reference (h) which is tabulated herein on Figure 4 in Table 4 of Appendix A that follows this discussion. And thermal properties of the test-radome material (Pyroceram 9606) are quoted from Reference (g) in Table 3 of Appendix A on the thermal-mass-center evaluations.

The methods of analysis that were used in sequence are as follows:

(1) The temperature data plotted on Figures 1-a and 1-c were analyzed by minimization of the squared-error functions.

(2) With the outer-surface temperatures (T_a) found in step (1) together with those cited in Reference (i) (which are plotted in Figures 1-b and 1-e), the regression curve shown in Figure 1 was obtained by minimizing the squared-error function.

(3) The inner-surface temperature equation (T_s, Figure 2) was derived from the test data plotted on Figures 1-d and 1-e along with the T_s values from step (1).

Table 1. Coordinates of Von Karman Test Radome.

Tip dist. to outer surf. (in.)	r_a (in.)	ψ (deg-min-sec)	sin ψ	cos ψ	Tip dist. to ctr. surf. (in.)	Tip dist. to inner surf. (in.)
0	0	0	0	1	0.1669	0.3338
0.06	0.0868	42-38-42	0.677,454	0.735,567	--	--
.105	.1321	46-40-53	.727,545	.686,056	.1908	--
.1742	.1924	50-19-12	.769,626	.638,480	.2350	.3338
.1824	.1999	50-37-07	.772,942	.634,482	.2617	.3410
.2825	.2773	53-41-17	.805,807	.592,184	.3565	.4305
.34	.3185	54-57-52	.818,797	.574,083	.4118	.4835
.3743	.3424	55-37-41	.825,389	.564,566	.4449	.5154
.45	.3929	56-52-18	.837,449	.546,516	.5183	.5866
.5743	.4715	58-29-18	.852,536	.522,674	.6396	.7050
.8	.6037	60-37-54	.871,487	.490,423	.8613	.9226
.9357	.6788	61-37-42	.879,889	.475,186	.9951	1.0545
1	.7128	62-02	.883,22	.468,96	1.0586	1.1172
1.3167	.8748	63-43-59	.896,738	.442,555	1.3720	1.4273
1.644	1.0315	65-04-03	.906,807	.421,545	1.697	1.75
2	1.1924	66-13	.915,08	.403,28	2.0504	2.1008
3	1.6072	68-34	.930,84	.365,42	3.0457	3.0914
4	1.9828	70-12	.940,88	.338,74	4.0423	4.0847
5	2.3304	71-27	.948,05	.318,13	5.0398	5.0795
7.075	2.9845	73-26-14	.958,51	.285,06	7.1106	7.1463
14.15	4.7730	77-52-50	.977,51	.209,95	14.1762	14.2025
16.3635	5.2345	79-03-45	.981,835	.189,74	16.3872	16.4109
21.225	6.0543	81-39-54	.989,42	.145,07	21.2431	21.2613
24	6.4184	83-27-35	.993,493	.113,900	24.0142	24.0285
28.3	6.75	90	1	0	28.3	28.3

Table 2. Computed and Measured Temperatures for 28.3" x 6.75" Von Karman Test Radome

Tip dist. to outer surf.	0"		0.94"		1"		1.32"	
x	T(°F)		T(°F)		T(°F)		T(°F)	
(thk. ratio)	Ref. (h)*	Eq (4)	Ref. (h)*	Eq (5)	Ref. (i)	Eq (6)	Ref. (h)*	Eq (7)
+ 1		1319		956	950	951		920
+ 0.90	1,228		916				879	
+ .75		973		694		689		669
+ .50		702		493	610	491		475
+ .25	498	499	343	342		341	331	331
0		352		239	355	238		231
- .25	210	253	160	172		171	156	167
- .50		196		133	205	133		129
- .75		167	122	116		116	119	113
- 1		160		113	155	112		109

Tip dist. to outer surf.	1.644"		2"		24"		
x	T(°F)		T(°F)		T(°F)		
(thk. ratio)	Exp.**	Eq (8)	Ref. (i)	Eq (9)	Exp.**	Ref. (i)	Eq (10)
+ 1		899	880	881		570	648
+ 0.75		653		641			483
+ .50		464	552	457		345	353
+ .25		324		319			254
0		226	320	223		202	182
- .25		163		161			134
- .50		126	182	125		118	105
- .75		109		109			91
- 1	106	106	136	105	87	95	87

* Reference (h) data are shown herein on Figure 4 in Table 4 of Appendix A.

** These measured temperatures are reported in Reference (i) for OAL wind-tunnel test No. 6053 at four seconds.

(4) The central-surface temperatures (T_c) computed in step (1) were analyzed by minimizing the squared-error function to find the regression formula that is shown in Figure 3.

(5) The single function $T = T_a f(x)$ of equations (22) and (23) was developed by statistical analysis of all of the temperatures secured from steps (1) to (4), inclusive, and is shown in Figures 1 to 4, inclusive.

It was found generally that the regression formulas, equations (4) to (10), (14) to (16), and (18) to (22), inclusive, are in good agreement with the analytical values from References (f) and (h) and the test data from Reference (i) which were reported to have computational and experimental-error ranges within ±7 percent.

The computed wall interior temperatures from Reference (i) appear to be high. The inner-surface values at 1.12 and 2.10 inches from the tip are 46 and 28 percent above the measured temperature of 106°F at 1.75 inches from the tip, and they are 38 and 30 percent higher than the regression values at the 1.12 and 2.10 inch locations (Table 2, where the outer-surface tip distances are given as 1, 2, and 1.644 inches for the above mentioned inner-surface points). At 24 inches from the tip, the analytical value is about 9 percent above the measured temperature of 87°F (Table 2). Such higher values can result from the use of coefficients of thermal conductivity (Table 3) that vary insufficiently with the Pyroceram wall temperature.

Overall, it is observed that the general equations derived in Reference (a), such as equations (1) and (2) in the present text, provide an excellent means for correlation and functional representation of the temperature distributions when employed with empirical coefficients obtained from numerical flow calculations that include the exchange of heat from air to wall through the boundary layer and heat conduction in the wall toward the base of the radome.

CONCLUSIONS

It is concluded that the temperature functions deriving from this investigation are suitable for evaluations of radome thermal stresses. Furthermore, they provide the only means now available to us for the correlation of ogive and Von Karman radome thermal-stress analyses in addition to being used in correlating test results and theory.

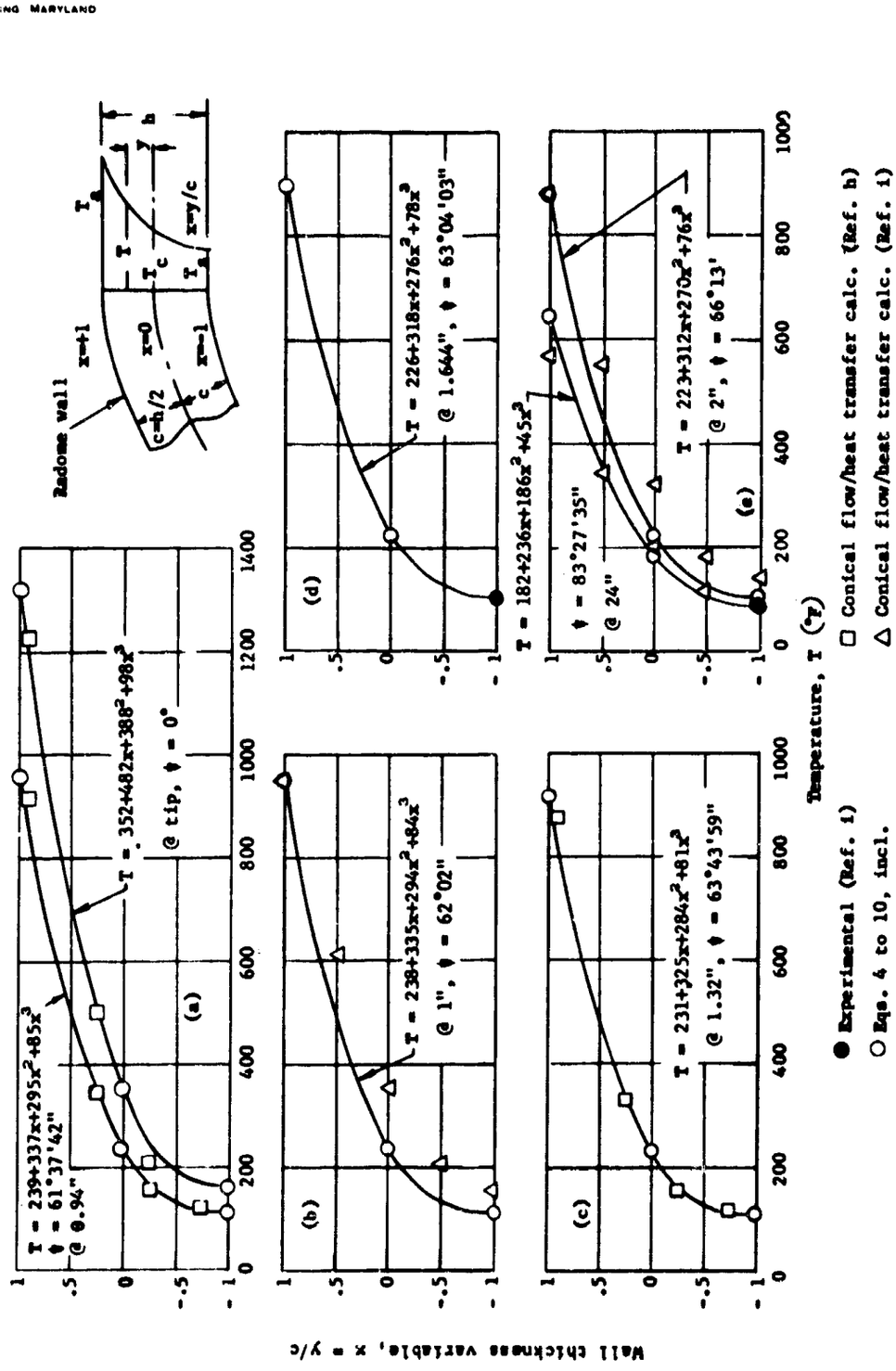

Fig. 1 WALL THICKNESS DISTRIBUTIONS OF TEMPERATURE FOR 28.3" x 6.75" VON KARMAN RADOME

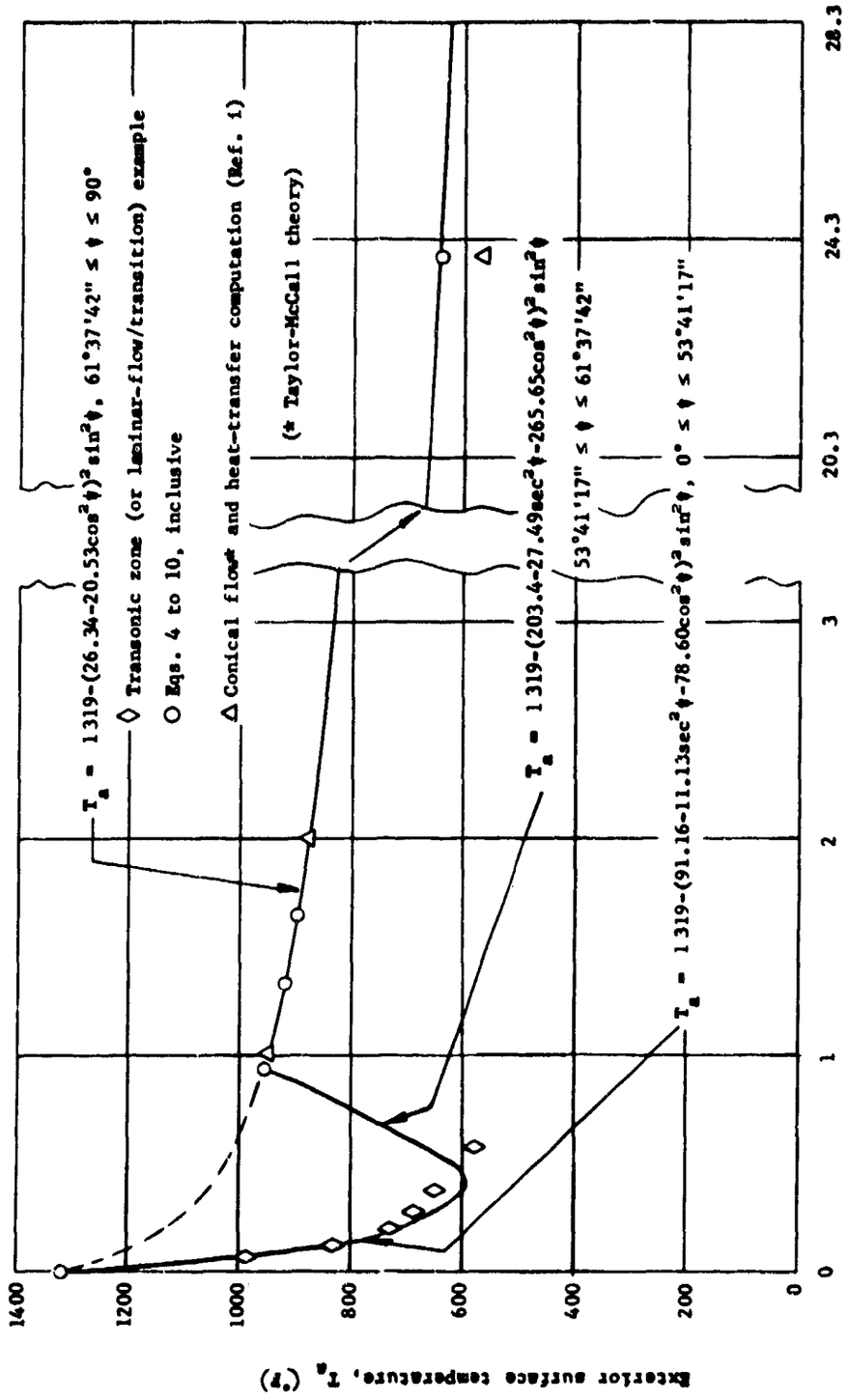

Fig. 2 TEMPERATURE DISTRIBUTION ALONG OUTER SURFACE OF 28.3" x 6.75" VON KARMAN RADOME

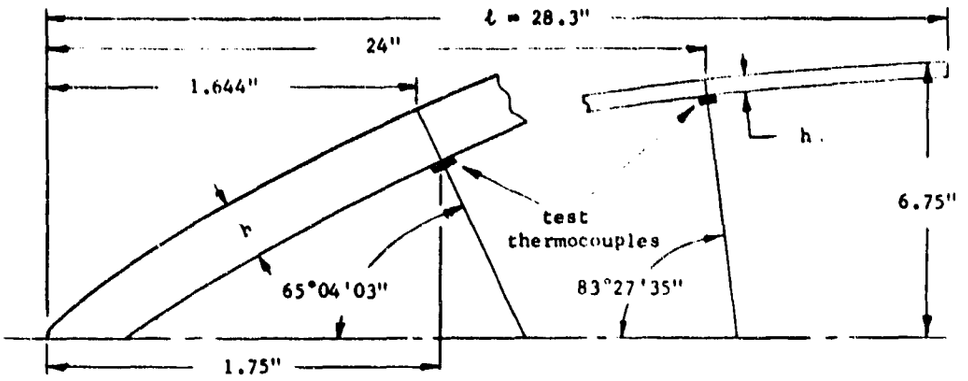

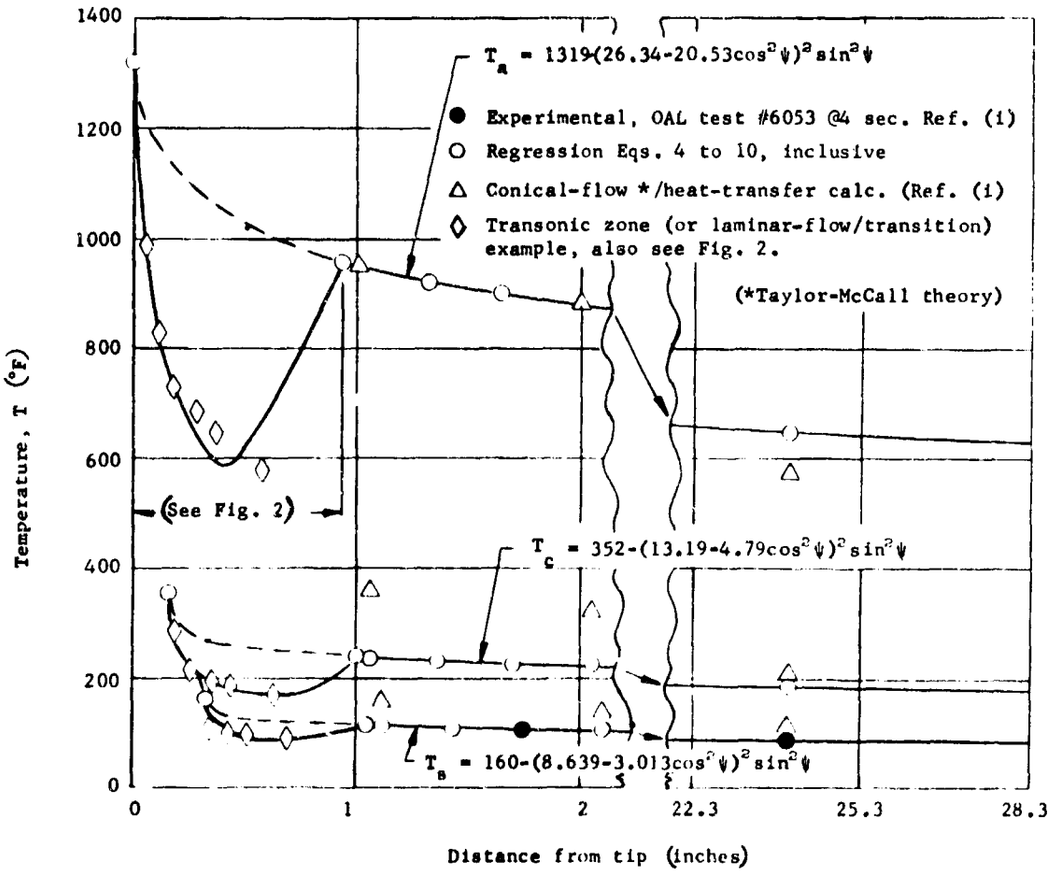

Fig. 3 EXTERIOR, CENTRAL, AND INTERIOR SURFACE SPANWISE TEMPERATURE DISTRIBUTIONS FOR 28.3"x 6.75" VON KARMAN TEST RADOME

APPENDIX A. Thermal-Mass Centers of Volume Segments.

The computer program of Reference (h) was set up for numerical analysis of the transfer of heat from air to wall and along the wall toward the radome base for the finite volume segments that are identified in Figure 4. The temperatures listed in Table 4 that resulted from the computer program were obtained as constants within their respective volume elements. There is one point in each finite increment of volume where the constant, or volume average, temperature equals the true wall value at the same point, and it is the thermal-mass-center of the element of volume. A few of these were evaluated to ascertain their effect on the temperature distribution.

The thermal-mass center can be located with the ratio $\bar{x}_t$, where $x = y/c$ is defined by the sketch in the upper right-hand corner of Figure 1. The values of $\bar{y}_t$ can be computed from the following equations:

$$v = 2\pi \int_{\psi_1}^{\psi_2} \int_{R_1}^{R_2} rRd\psi dR \qquad (24)$$

$$\bar{k}\, v = 2\pi \int_{\psi_1}^{\psi_2} \int_{R_1}^{R_2} krRd\psi dR \qquad (25)$$

$$\bar{k}\, v\, \bar{y}_t = 2\pi \int_{\psi_1}^{\psi_2} \int_{R_1}^{R_2} ykrRd\psi dR \qquad (26)$$

where ψ_1 and ψ_2 are the values of the coordinate angle at the beginning and end, respectively, of the volume element; R_1 and R_2 are the radial coordinates of the lower and upper surfaces (Figure 4), respectively, of the volume element; v is the volume in cubic inches; k is the temperature-dependent coefficient of thermal conductivity (Table 3); and r is the cross-sectional radius measured vertically from

Table 3. Variations with Temperature of Thermal Properties of Pyroceram 9606

T (°F)	k (Btu/ft-hr-°F)	c_p (Btu/lb-°F)
77	2.661	0.210
122	2.492	.215
212	2.322	.223
392	2.105	.234
572	1.911	.244
752	1.790	.253
932	1.742	.262
1,292	1.717	.277

(1) Over the above temperature range, the unit weight remains constant at 162.3 pcf.

(2) k = coefficient of thermal conductivity.

(3) c_p = specific heat at constant pressure.

(4) The above tabulated data were obtained from Reference (g).

Note: Volume-element temperatures computed by conical-flow (Taylor-McCall theory) and heat-transfer analyses. They apply to OAL wind-tunnel test No. 6053 at 4 sec. (Refs. (f) & (i) give free-stream and total air properties as:

T_o = 362°F T_t = 1343°F

P_o = 2120 psf P_t = 213 psi

V_o = 3433 fps

M_o = 2.44

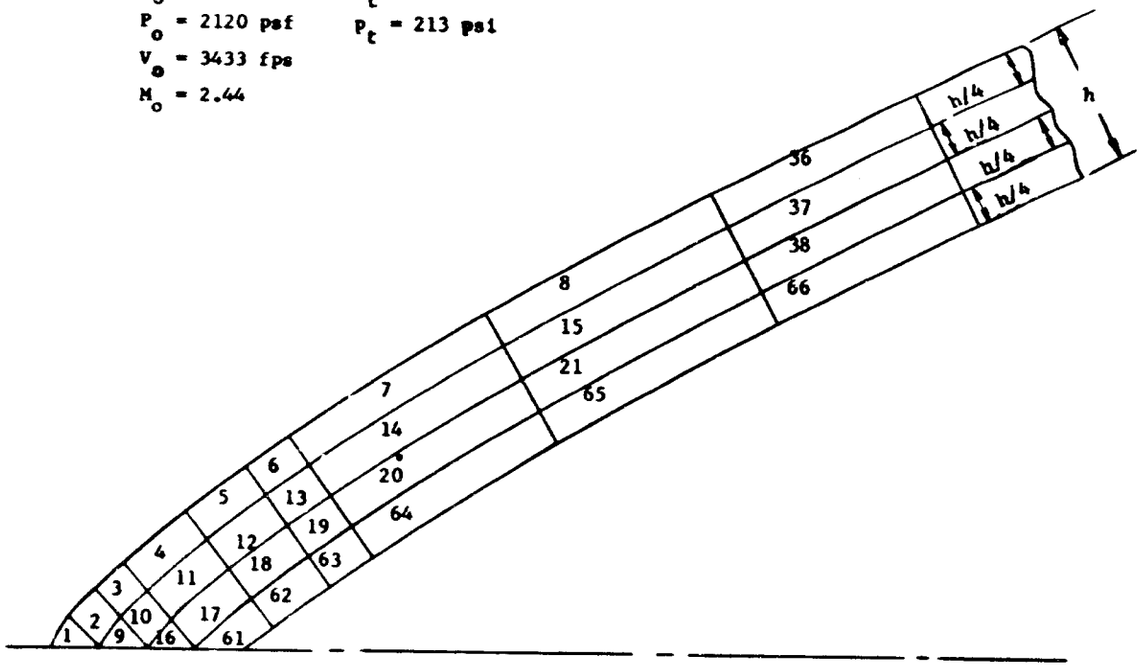

Selection and designation of volume elements

Table 4. Temperatures from APL Computer Program.

Element No.	T (°F)
1	1228
2	941
3	790
4	695
5	656
6	616
7	551
8	916
9	498
10	354
11	276
12	251
13	241
14	220
15	343
16	210
17	142
18	126
19	123
20	115
21	160
36	979
37	331
38	156
61	112
62	100
63	97
64	93
65	122
66	119

Fig. 4 TEMPERATURES CAUSED BY AERODYNAMIC HEATING OF 28.3" x 6.75" VON KARMAN RADOME

the longitudinal axis of the radome (also see References (b) and (d)). And with the foregoing relations, it was found that

	$\bar{x}_t$		$\bar{x}_t$
El. (1):	+ 0.903	El. (8):	+ 0.898
El. (9):	+ .253	El.(15):	+ .247
El.(16):	- .248	El.(21):	- .253
El.(61):	- .746	El.(65):	- .751

where "El. (No.)" refers to the numbered elements of volume shown in Figure 4. Changes in the above values are slight, and the computed temperatures were plotted at +0.90, ±0.25, and -0.75.

APPENDIX B. Revised Thermal-Mass Center Calculations.

The method of finding the thermal-mass center to locate the position of a constant temperature that is calculated as an average value in a volume segment is revised. The revision is compared with the method of Appendix A that was employed in the temperature-distribution investigation in the text; and it was found that the difference between the two methods affected the results to a negligible extent.* There may be other cases, however, where the difference becomes significant. Therefore, the new method is recommended for use in future studies that are similar to the present investigation.

In the text, the experimental and theoretical temperature data were plotted at the thermal-mass-centers of the volume segments of the test radome wall. These mass-center locations were based on the heat variant coefficient of thermal conductivity (k) given in Appendix A.

Upon further consideration of the problem, we observed that this method leads to location of a volume-average value of k, which does not necessarily coincide with the position of the volume-average temperature. Calculation of the mass-center position of the average temperature is discussed in subsequent parts of the present appendix.

The computer program of Reference (h) was set up for numerical analysis of the transfer of heat from air to wall and through the wall interior toward the radome base for the volume elements that are identified in Figure 4. The temperatures listed in Table 4 that resulted from the computer program were obtained as constants within their respective volume elements. There is one point in each finite increment of volume where the constant, or volume-average, value equals the true wall temperature at the same point, and it is the thermal-mass-center of the element of volume. A few of these were evaluated to ascertain their effect on the temperature distribution.

The thermal-mass-center can be located with the ratio $\bar{x}_t$, where x=y/c is defined in the nomenclature listing. The values of $\bar{y}_t$ are computed with the following equations:

---

* The effect amounted to less than 0.1 percent.

THE JOHNS HOPKINS UNIVERSITY
APPLIED PHYSICS LABORATORY
SILVER SPRING, MARYLAND

$$v = 2\pi \int_{\psi_1}^{\psi_2} \int_{R_1}^{R_2} rRd\psi dR \qquad (27)$$

$$vT_{av} = 2\pi \int_{\psi_1}^{\psi_2} \int_{R_1}^{R_2} TrRd\psi dR \qquad (28)$$

$$vr_{av}\bar{y}_t = 2\pi \int_{\psi_1}^{\psi_2} \int_{R_1}^{R_2} RyTrd\psi dR \qquad (29)$$

where ψ_1 and ψ_2 are the values of the coordinate angle at the beginning and end, respectively, of the volume element; R_1 and R_2 are the radial coordinates of the lower and upper surfaces (Figure 4), respectively, of the volume element; v is the volume in cubic inches; T equals the temperature at any point in the segment of volume; and r is the cross-sectional radius measured vertically from the longitudinal axis of the radome. With the foregoing [illegible]ions and temperature data from the text, it was found that

	$\bar{x}_t$		$\bar{x}_t$
El. (1):	+ 0.906	El. (8):	+ 0.895
El. (9):	+ .254	El.(15):	+ .252
El.(16):	- .242	El.(21):	- .246
El.(61):	- .748	El.(65):	- .751

where "El. (No.)" refers to the numbered elements of volume shown in Figure 4.

The preceding numerical values of $\bar{x}_t$ were used to check the results that are reported herein, and it was learned that they produce a negligible effect (less than 0.1 percent). Nevertheless, equations (1) to (3), inclusive, are the correct ones to use for plotting the volume-average temperatures; and future cases may come up wherein it is essential to use them in preference to equations (24), (25), and (26) of Appendix A. We recommend their adoption, therefore, for the purpose at hand.

REFERENCES

(a) M. B. Tate, "Air Properties and Flow Conditions Around the Nose of a Bount Radome" (Unclassified), APL/JHU TG-981 (to be published).

(b) M. B. Tate, "Large Axisymmetric Thermal Bending Stresses in Ogival Radomes with Heat Variant Material Properties" (Unclassified), APL/BBE EM-3995, 1965.

(c) M. B. Tate, "Functionalization of Pyroceram 9606 Test Data for Radome Thermal-Stress Analysis" (Unclassified), APL/JHU TG-980 (to be published).

(d) M. B. Tate, "Curvature Radii and Derivatives for Thermal-Stress Analysis of Von Karman Radomes " (Confidential), APL/JHU TG-982 (to be published).

(e) H. W. Liepmann and A. Roshko, "Elements of Gas Dynamics," 2d ed, Wiley, New York, 1967.

(f) R. P. Suess, "Comparison of Theoretical and Experimental Radome Temperatures and Stresses" (Confidential), APL/BBE EM-3884, 1964.

(g) R. P. Suess, "Thermal Analysis of Pointed and Blunted Radomes for TYPHON MR and TYPHON IR " (Confidential), APL/BBE EM-3687, 1963.

(h) R. P. Suess, "IBM 7094 Computer Program for the Computation of Radome Thermal Stresses" (Unclassified), APL/BBE EM-3854, 1964.

(i) D. A. Maytubby, "Final Test Results from the Standard Missile Type 1 (ER) and the Medium Range TYPHON Wind Tunnel Test Program for the Radome Assemblies" (Confidential), TM 6-332-298, GD/Pomona, 1965.

UNCLASSIFIED
Security Classification

DOCUMENT CONTROL DATA - R & D

Security classification of title, body of abstract and indexing annotation must be entered when the overall report is classified)

1. ORIGINATING ACTIVITY (Corporate author)	2a. REPORT SECURITY CLASSIFICATION
The Johns Hopkins Univ., Applied Physics Lab. 8621 Georgia Ave. Silver Spring, Md.	Unclassified 2b. GROUP N.A.

3. REPORT TITLE

Statistical Analysis of Temperature Data from Wind Tunnel Test of a Von Karman Radome

4. DESCRIPTIVE NOTES (Type of report and inclusive dates)
Technical Memorandum

5. AUTHOR(S) (First name, middle initial, last name)

Manford B. Tate

6. REPORT DATE	7a. TOTAL NO. OF PAGES	7b. NO. OF REFS
March 1968	21	9

8a. CONTRACT OR GRANT NO	9a. ORIGINATOR'S REPORT NUMBER(S)
NOw 62-0604 c b. PROJECT NO.	TG-983
c.	9b. OTHER REPORT NO(S) (Any other numbers that may be assigned this report)
d.	

10. DISTRIBUTION STATEMENT

This document has been approved for public release and sale; its distribution is unlimited.

11. SUPPLEMENTARY NOTES	12. SPONSORING MILITARY ACTIVITY
	NAVORDSYSCOM

13. ABSTRACT

Temperatures obtained from an Ordnance Aerophysics Laboratory wind-tunnel test on a Von Karman radome are studied and put into functional form for theoretical analysis of radome thermal stresses. It was found that the radome wall temperature can be expressed analytically by a single function that defines the temperatures at all points in the wall except for a short length near the tip for which another expression is developed. The single function is further separable by variables into two functions, one of which describes the spanwise distribution and the other, the wall-thickness distribution of the temperature. This finding is highly advantageous mathematically. The analytical and test results are presented and compared in three figures and recorded in two tables. Good agreement between experiment and analysis was found to exist with the difference range generally not in excess of approximately ±7 percent while being less than half this amount in most cases. The derived function overestimates the maximum temperatures by about 0.5 percent, but this is a conservative feature insofar as the theoretical prediction of thermal stress is concerned. The range of experimental error in the original data was reported by the test engineers to be also about ±7 percent.

DD FORM 1 NOV 65 1473

UNCLASSIFIED
Security Classification

14. KEY WORDS

Radome temperature test data
Analysis of temperature test data
Wind tunnel test of Von Karman radome
Von Karman radome thermal data
Empirical distribution of radome temperatures